Chemical Science



EDGE ARTICLE

View Article Online
View Journal | View Issue



Cite this: Chem. Sci., 2024, 15, 10193

d All publication charges for this article have been paid for by the Royal Society of Chemistry

Received 18th April 2024 Accepted 25th May 2024

DOI: 10.1039/d4sc02569e

rsc li/chemical-science

Crystal clear: unveiling giant birefringence in organic-inorganic cocrystals†

Yang Li and Kang Min Ok *

Coplanar groups with large anisotropic polarizability are suitable as birefringence-active groups for investigating compounds with significant birefringence. In this study, the organic coplanar raw reagent, $o-C_5H_5NO$ (4HP), was selected as an individual complement. Utilizing the cocrystal engineering strategy, we successfully designed two cocrystals: $[LiNO_3 \cdot H_2O \cdot 4HP] \cdot 4HP$ (Li-4HP2) and $[Mg(NO_3)_2 \cdot 6H_2O] \cdot (4HP)_2$ (Mg-4HP), and one by-product: $LiNO_3 \cdot H_2O \cdot 4HP$ (Li-4HP), which were grown using a mild aquasolution method. The synergy of the coplanar groups of NO_3^- and 4HP in the structures resulted in unexpectedly large birefringence values of 0.376-0.522@546 nm. Furthermore, the compounds exhibit large bandgaps (4.08–4.51 eV), short UV cutoff edges (275–278 nm), and favorable growth habits, suggesting their potential as short-wave UV birefringent materials.

Introduction

Cocrystals are an important class of compounds with unique properties, widely utilized in ferroelectricity, ambipolar charge transport, photovoltaics, *etc.*¹⁻⁵ In general, noncovalent interactions assemble neutral molecules in a stoichiometric ratio to construct the cocrystal, which is beneficial for synthesizing the cocrystal under mild conditions. In addition, the facile selection of components could effectively design and tune the structure and properties of the target cocrystal.⁶⁻⁸ Therefore, the cocrystal engineering strategy has been proposed and widely applied to investigate and grow large sized new nonlinear optical/birefringent materials, including compounds in the AX·H₃C₃-N₃O₃ family,⁹⁻¹¹ KF·B(OH)₃,¹² RbCl·H₂SeO₃,¹³ (NH₄HCOO)₃[-B(OH)₃]₂,¹⁴ KNO₃·NH₃SO₃,¹⁵ KIO₃·Te(OH)₆,¹⁶ K₂SO₄·(SbF₃)₂,¹⁷ and K₂SO₄·HIO₃.¹⁸

Birefringent crystals can modulate and control light polarization, making them extensively utilized in laser-related fields.
¹⁹⁻²³ Commercial birefringent materials, such as MgF₂, α -BaB₂O₄ (α -BBO), CaCO₃, TiO₂, and LiNbO₃, play critical roles across the deep ultraviolet (DUV) to near-infrared (NIR) regions.
²⁴⁻²⁸ However, distinct limitations, such as the phase transition in α -BBO and the difficulty in growing high-quality CaCO₃ crystals, make exploring new birefringent materials with substantial birefringence in the short-wave UV region an urgent and significant endeavor.

Department of Chemistry, Sogang University, Seoul 04107, Republic of Korea. E-mail: kmok@sogang.ac.kr

† Electronic supplementary information (ESI) available: Crystallographic data, IR spectra, TGA diagrams, band structures, and ELF diagrams. CCDC 2346368, 2346369 and 2303329. For ESI and crystallographic data in CIF or other electronic format see DOI: https://doi.org/10.1039/d4sc02569e

Birefringence-active groups with large anisotropic polarizability $(\Delta \alpha)$ are the cornerstone for designing birefringent materials.29 π-Conjugated groups with delocalized electrons and cations with lone pair electrons exhibit large $\Delta \alpha$, making them suitable birefringence-active groups.30-34 In contrast, the nearly isotropic distribution of electronic clouds in halogens results in rigid regular tetrahedral groups such as TO_4 (T = B, Si, P, S, etc.) having $\Delta \alpha$ close to zero.³⁵ Hence, π -conjugated systems such as MO₃ (M = B, C, and N) groups, and benzenelike six-membered ring groups (B₃O₆) are among the hotspots for investigating birefringent materials.36-40 Consequently, classical birefringent materials including α-BBO,25 CaCO3,26 and NaNO₃ have been investigated. ⁴¹ Among the MO₃ (M = B, C, and N) family, NO₃ exhibits the shortest bond length, indicating a more substantial overlap between N 2p and O 2p orbitals. This overlap results in heightened p_{π} - p_{π} interactions, yielding the largest Δα within the MO₃ family.⁴² Besides, B₃O₆, composed of three BO₃ units, attains a '1 + 1 + 1 > 3' configuration, affirming the suitability of six-membered rings as birefringence-active groups.42

Recent research has expanded exploration from the traditional inorganic π -conjugated system to the organic system.⁴³ Organic six-membered ring groups (6-MRs) have been identified as excellent birefringence-active groups with considerably larger $\Delta \alpha$, such as $[H_x C_3 N_3 O_3]^{(3-x)-}$ (x=0–3) and $C_3 N_6 H_7^{+,44-47}$ As a result, organic 6-MR compounds with substantial birefringence have been reported.^{48–50}

However, although NO_3^- and organic 6-MRs have attractive $\Delta \alpha$, these groups will red-shift the bandgaps, posing an obstacle to their potential application in the UV region. Therefore, it is still necessary to introduce alkali and alkaline earth metal cations without d-d/f-f electron transitions to enlarge the bandgap.

Strong covalent cations including Li^+ and Mg^{2+} draw our attention due to the benefits of enlarging bandgaps. Besides, they can easily form hydrate cations in the water solution system: for example, Mg^{2+} tends to form the hydrated $[Mg(H_2O)_6]^{2+}$, which could serve as a good hydrogen bonding donor to govern the distribution of NO_3^- and oxygen heterocycle groups and construct the cocrystal.

Inspired by the above ideas, we decided to explore the Li/Mg-NO₃-4HP system for hybrid organic–inorganic cocrystals with giant birefringence. Using the cocrystal approach, LiNO₃·H₂-O·4HP (Li-4HP), [LiNO₃·H₂O·4HP]·4HP (Li-4HP2), and [Mg(NO₃)₂·6H₂O]·(4HP)₂ (Mg-4HP) were grown νia the mild slow evaporation method. They exhibit short UV cutoff edges (275–278 nm) and giant birefringence (0.376–0.522@546 nm), thus being promising short-wave UV birefringent crystals. Li-4HP2 demonstrates a giant birefringence of 0.522@546 nm, which is the largest among those reported for inorganic–organic hybrid cocrystals in the short-wave UV region. This study serves an exemplary illustration of successful exploration into novel short-wave UV birefringent crystals with giant birefringence and wide bandgaps using the cocrystal approach.

Experimental section

Single crystals of compounds Li-4HP, Li-4HP2, and Mg-4HP were grown via the aqua-solution method at room temperature. LiNO $_3$ (Sigma, 10 mmol) and 4HP (TCI, >99%, 10 mmol) were used for Li-4HP, with the 4HP amount increased to 20 mmol for Li-4HP2. A mixture of Mg(NO $_3$) $_2 \cdot 6H_2O$ (DAEJUNG, 98%, 10 mmol) and 4HP (20 mmol) was used for Mg-4HP. After one week, colorless bulk crystals of Li-4HP2 and Mg-4HP (with sizes up to $2 \times 1 \times 0.5 \text{ cm}^3$) and millimeter-level needle-like crystals of Li-4HP were obtained. These crystals were washed with distilled water for subsequent measurements. The polycrystalline samples were prepared by directly grinding the as-grown crystals and checked using powder X-ray diffraction.

The powder X-ray diffraction data were collected *via* the Mini Flex 600 diffractometer using Cu K α ($\lambda = 1.54406$ Å) radiation with 40 kV and 15 mA at room temperature. The sample was scanned in the 2θ range of 5–70° at a scan speed of 10° min⁻¹ and a scan step width of 0.02°. The measured diffraction pattern of the title compounds matched well with the simulated one (Fig. S1 and S4†).

The crystal structures were determined via a Bruker D8 QUEST diffractometer with a Mo K α radiation source ($\lambda=0.71073$ Å) at the Advanced Bio-Interface Core Research Facility at Sogang University at room temperature. The SAINT and SADABS programs were used for data reduction and absorption correction, respectively. ⁵¹ The OLEX2 package was used to solve and refine the structure. ⁵² Solved structures were checked using PLATON to avoid any missing higher symmetry. ⁵³ Crystallographic data, structure refinement information, atomic coordinates, equivalent isotropic displacement parameters, selected bond lengths, and bond angle are listed in the ESI (Tables S1–S5).†

Infrared (IR) spectra were recorded using a Thermo Scientific Nicolet iS50 FT-IR spectrometer. The ground sample was placed on the diamond attenuated total reflectance crystal (Fig. S2†).

The ultraviolet-visible-near infrared (UV-vis-NIR) transmittance spectrum for Mg-4HP was obtained using a Shimadzu SolidSpec-3700 DUV spectrophotometer at room temperature in the 200–1600 nm wavelength range. The UV-vis diffuse-reflectance spectra for Li-4HP, Li-4HP2 and Mg-4HP, and 4HP were recorded on a Lambda 1050 scan UV-vis spectrophotometer at room temperature, covering the spectral range of 200–800 nm.

Thermogravimetric analysis (TGA) was conducted using a SCINCO TGA-N 1000 thermal analyzer. The ground polycrystalline samples were loaded into alumina crucibles and heated to 900 °C at a rate of 10 °C min⁻¹ under flowing air (Fig. S3†).

Single crystals of **Li-4HP2** (0.0469 g) and **Mg-4HP** (1.1771 g), and a polycrystalline sample of **Li-4HP** (0.6125 g) were used to quantify the change in weight after exposure to air over seven days. The ambient temperature and humidity were maintained at 25 \pm 5 °C and 36 \pm 5%, respectively.

The polarizability anisotropy for NO₃⁻ and 4HP was calculated using Gaussian 09 at the B3LYP/6-31G level and analyzed by Multiwfn.54,55 CP2K (version 2022.1) was applied to calculate the electron localization function (ELF) at the B3LYP/6-311G* level (Fig. S5†).56 The CASTEP package (version 23.1) was utilized for the first-principles calculations based on densityfunctional theory.⁵⁷ Band structure, density of states, and optical properties were calculated using the Perdew-Burke-Ernzerhof (PBE) generalized gradient approximation (GGA) and the norm-conserving pseudopotential (NCP).58-61 The valence electrons (cutoff energy) of the pseudo-potential used are as follows: H 1s1 (650 eV), C 2s22p2 (680 eV), N 2s22p3 (700 eV), O $2s^22p^4$ (750 eV), Li $2s^1$ (450 eV), and Mg $2s^22p^63s^2$ (900 eV). A plane-wave cut-off energy of 990 eV for Mg-4HP and Mg(NO₃)₂·6H₂O, and 830 eV for Li-4HP and Li-4HP2 were chosen. A dense k-point sampling of less than 0.04 Å^{-1} was adopted for geometry optimization and calculation of optical properties (Fig. S6-S7†). Other parameters were set at the ultrafine level as default.

Results and discussion

Li-4HP crystallizes in the monoclinic space group, $P2_1/n$ (no. 14) with unit cell parameters of a = 8.821(8) Å, b = 10.477(9) Å, c =9.205(9) Å, $\beta = 110.89(3)^{\circ}$, and $V = 794.8 \text{ Å}^3$. Li⁺ is fivecoordinated with oxygen atoms and generated the $[\text{LiO}_4\text{H}_2\text{O}]^{7-}$ polyhedra. The $[\text{LiO}_4\text{H}_2\text{O}]^{7-}$ polyhedra are cornersharing the O1 atom with 4HP, edge-sharing the O3 and O4 atoms with NO₃, and edge-sharing the O1-O1 with the adjacent $[\text{LiO}_4\text{H}_2\text{O}]^{7-}$ polyhedra to form the $[\text{LiNO}_3\cdot\text{H}_2\text{O}\cdot\text{4HP}]_2$ dimer (Fig. 1a). In the dimer, the distances between Li and O, and between N and O, are in the ranges of 1.940 to 2.552 Å and 1.244 to 1.252 Å, respectively. The dihedral angle between 4HP and NO₃⁻ is 85.06° (Fig. S8†). This nearly vertical arrangement benefits the dimer further by connecting adjacent [LiNO₃·H₂-O·4HP]2 dimers through hydrogen bonds of O/N-H···O, generating pseudo-layers of $\{[LiNO_3 \cdot H_2O \cdot 4HP]_2\}^0$ in the ac plane (Fig. 1b). The dihedral angle between adjacent pseudolayers (A and B) is 87.88°. These pseudo-layers further stack

Edge Article Chemical Science

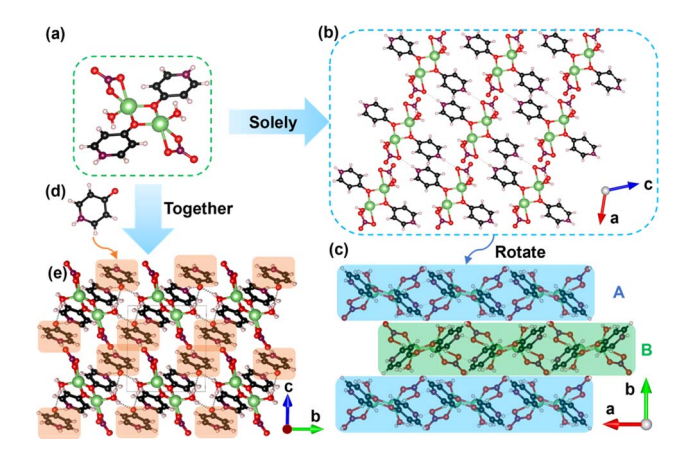


Fig. 1 Ball-and-stick representations of (a) the [LiNO₃·H₂O·4HP]₂ dimer and pseudo-layers of $\{[LiNO_3 \cdot H_2O \cdot 4HP]_2\}^0$ viewed along (b) the b-axis and (c) c-axis for Li-4HP. (d and e) The additional neutral 4HP separates the [LiNO₃·H₂O·4HP]₂ dimers and generates a pseudothree-dimensional structure of Li-4HP2 (black, C; purple, N; red, O; white, H; green, Li).

along the b-axis with an ABAB arrangement, generating the final pseudo-two-dimensional structure (Fig. 1c).

Li-4HP2 crystallizes in the triclinic space group, $P\bar{1}$ (no. 2) with unit cell parameters of a = 8.2120(6) Å, b = 8.9624(6) Å, c =9.9320(7) Å, $\alpha = 82.101(2)^{\circ}$, $\beta = 106.673(2)^{\circ}$, $\gamma = 70.184(2)^{\circ}$, and $V = 638.59 \text{ Å}^3$. As depicted in the formula, it is composed of the [LiNO₃·H₂O·4HP]₂ dimer and one additional 4HP (Fig. 1a and d). With the additional 4HP introduced into the lattice, the dihedral angle between 4HP and NO₃ in the [LiNO₃·H₂- $O\cdot 4HP$ ₂ dimer was decreased from 85.06° to 32.03° (Fig. S8†). Among the [LiNO₃·H₂O·4HP]₂ dimer, the bond lengths of Li-O range from 1.935 to 2.333 Å, and the distances between N and O atoms range from 1.246 to 1.252 Å. It should be noticed that in Li-4HP2, adjacent [LiNO₃·H₂O·4HP]₂ dimers are assembled, generating the pseudo-layers of $\{[LiNO_3 \cdot H_2O \cdot 4HP]_2\}^0$. However, in Li-4HP2, the additional neutral 4HP separates these [LiNO₃·H₂O·4HP]₂ dimers and generates the final pseudothree-dimensional structure (Fig. 1e). Interestingly, the 4HP is nearly parallel to the distribution of the structure, indicating that the individual 4HP plays a key role in governing the arrangements of coplanar groups in Li-4HP2.

Mg-4HP crystallizes in the monoclinic space group, I2/a (no. 15) with unit cell parameters of a = 24.6517(11) Å, b = 6.4107(3)Å, c = 26.2782(12) Å, $\beta = 106.673(2)^{\circ}$, and V = 3978.27 Å³. An asymmetric unit consists of one [Mg(H₂O)₆]²⁺ octahedron, two NO₃ groups, and 4HP groups, which agrees with the chemical formula (Fig. 2b-d). The Mg-O distances range from 2.032 to 2.080 Å, and the corresponding distortion (Δd) is 0.089. Thus, weak distortion makes little contribution to the birefringence. The distances between N and O atoms in the NO₃ groups range from 1.221 to 1.259 Å. The bond lengths of C-O and C-N fall into the range of 1.278 to 1.282 Å and 1.333 to 1.345 Å, respectively, matching well with reported compounds. Hydrogen bonds of O-H···O were observed among the $[Mg(H_2O)_6]^{2+}$ octahedron, coplanar NO_3^- and 4HP groups. Hydrogen bonding interactions between N2-H2 in 4HP and

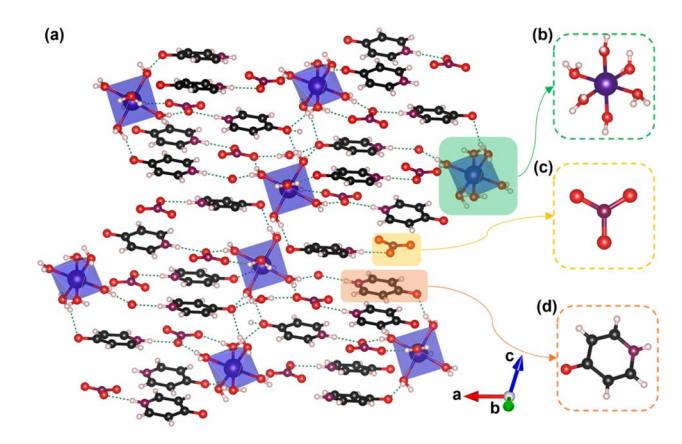


Fig. 2 Ball-and-stick and polyhedral representations of (a) Mg-4HP viewed along the b-axis (black, C; purple, N; red, O; blue, Mg; white, H). (b) $[Mg(H_2O)_6]^{2+}$, (c) NO_3^- , and (d) 4HP groups are highlighted.

O13-N3 from NO₃ were observed, generating the $[(NO_3)\cdot(4HP)]^-$ dimer. The NO_3^- and 4HP are nearly parallel in the dimer, and the dihedral angles range from 1.45 to 14.88° (Fig. S9†). The hydrogen bonds further assemble this dimer and the $[Mg(H_2O)_6]^{2+}$ octahedron, constructing the final pseudothree-dimensional structure (Fig. 2a).

The IR spectra in Fig. S2† reveal the characteristic vibrations of 4HP ($\nu_{C=\!-\!O}$ at 1645 cm $^{-1}$, ν_{N-H} at 3230 cm $^{-1}$), MgO $_6$ (ν_{Mg-O} at 824 and 1402 cm⁻¹), H₂O (peak at 3411 cm⁻¹), and NO₃ (peaks at 850, 769 and 715 cm⁻¹), respectively.⁶²⁻⁶⁴

UV-vis diffuse reflectance spectra suggest that the compounds Li-4HP, Li-4HP2, Mg-4HP, and 4HP possess short UV cutoff edges of 276, 278, 275, and 291 nm, respectively (Fig. 3). A polished crystal of compound Mg-4HP with a suitable size was selected to measure the UV-vis-NIR transmittance spectrum (Fig. S10†). At 275 nm, the transmittance remains at 0.02%, which corresponds well to the diffuse reflectance result. The corresponding bandgaps are 4.08, 4.15, 4.51, and 3.95 eV for compounds Li-4HP, Li-4HP2, Mg-4HP, and 4HP, respectively

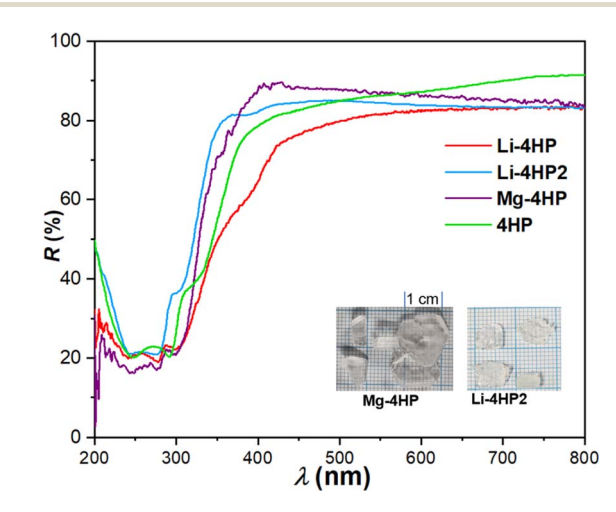


Fig. 3 UV-vis diffuse reflectance spectra for Li-4HP, Li-4HP2, Mg-4HP and 4HP. (Inset): As-grown crystals of Mg-4HP (left) and Li-4HP2 (right).

(Fig. S11†). Therefore, these three compounds, with broad bandgaps, could potentially be birefringent crystals applicable in the short-wave UV region.

Chemical Science

The thermal stability data indicate that during the heating of **Li-4HP, Li-4HP2**, and **Mg-4HP** from 25 to 900 °C, they lose water molecules in the first step (for **Li-4HP**, cal. 9.9%, exp. 9.9%; for **Li-4HP2**, cal. 6.5%, exp. 6.5%; for **Mg-4HP**, cal. 24.2%, exp. 22.8%). The subsequent step for **Li-4HP** and **Li-4HP2** involves the loss of CO₂, H₂O, and N₂, forming Li₂CO₃. The subsequent step involves the loss of the organic molecule **4HP** and nitrate, finally generating the corresponding oxides, Li₂O (for **Li-4HP**, cal. 8.2%, exp. 6.8%; for **Li-4HP2**, cal. 6.2%, exp. 7.4%) and MgO (for **Mg-4HP**, cal. 9.2%, exp. 11.7%) (Fig. S3†).

After exposure to air for seven days, Li-4HP, Li-4HP2, and Mg-4HP exhibited almost no change in mass. In addition, PXRD patterns measured after exposure to air for a week confirm that all the reported samples have good air stability under ambient temperature and humidity conditions (Fig. S4†). The band structures indicate that Li-4HP, Li-4HP2, and Mg-4HP belong to the class of direct bandgap compounds. The calculated bandgaps are 3.41, 3.47, and 3.11 eV, respectively, which are smaller than the experimental bandgaps (Fig. S6†). The differences were applied as scissor corrections to analyze the optical properties. In all three compounds, the upper regions of the valence band (VB) are mainly occupied by the C/N/O 2p states, with a small contribution from the H 1s states. The bottom of the conduction band (CB) consists of C/N/O 2p and Li 2p states (Li-4HP and Li-4HP2), respectively. These results suggest that the organic group of 4HP primarily determines the optical properties of these compounds (Fig. S7†). As revealed by the electron localization function (ELF) diagrams in Fig. S5,† delocalized π bonds were observed in the NO₃ and 4HP of both Li-4HP, Li-4HP2, and Mg-**4HP.** The synergistic effect of NO₃⁻ and **4HP** endows these compounds with giant optical anisotropy, as expected.

The relationship between wavelength and the birefringence is depicted in Fig. S12 and S13.† The calculated birefringence values for Li-4HP, Li-4HP2, and Mg-4HP are 0.387, 0.546, and 0.376 (0.227 on the (100) plane), respectively. Crystals of Li-4HP, Li-4HP2, and Mg-4HP (on the (100) plane) were measured using a cross-polarizing microscope. The optical path differences (R)at 546 nm are 3.620, 8.265, 1.799 µm, with thicknesses of 10, 15.823, and 7.951 μm (Fig. 5, S14 and S15†). Derived from the formula: $R = d \times \Delta n$, the birefringence at 546 nm is calculated as 0.362, 0.522, and 0.226, closely matching the calculated values of 0.387, 0.546, and 0.227. The measured birefringence of Mg-4HP is limited because the only natural crystal plane suitable for measurement is the (100) crystal plane, and thus it does not reach the largest birefringence of 0.376@546 nm. However, the measured value of 0.226@546 nm still fits the calculated birefringence on the (100) crystal plane well. Such giant birefringence is significantly larger than those of commercial birefringent materials such as α-BaB₂O₄ (0.122 @532 nm) and YVO₄ (0.225 @633 nm) (Fig. 4).25,65 Besides, Li-4HP2 exceeds other reported organic-inorganic hybrid cocrystals in the short-wave UV region. For example, $ANO_3 \cdot H_3C_3N_3O_3$ (A = K and Rb) has values ranging from 0.243 to 0.268 @546.1 nm,66 AX (H3C3N3- O_3 _x (A = alkali metal cations, X = Cl/Br/I, x = 1-2) ranges from

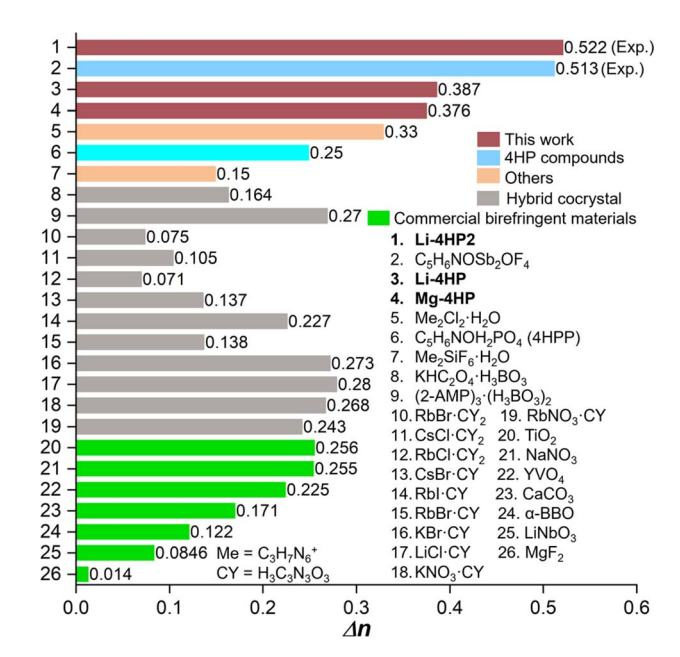


Fig. 4 Calculated (experimental) birefringence values for Li-4HP, Li-4HP2, and Mg-4HP (@546 nm) compared with reported values for other birefringent crystals.

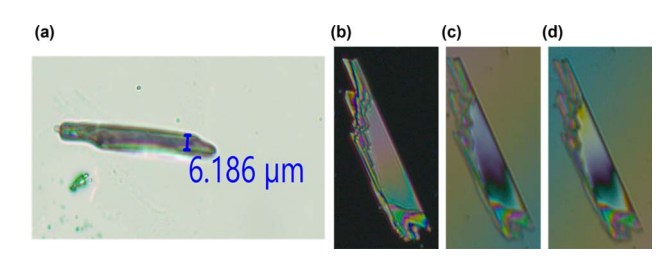


Fig. 5 (a) Thickness of a Li-4HP2 crystal and (b-d) a Li-4HP2 crystal observed under cross-polarized light, achieving complete extinction under a polarizing microscope.

0.071 to 0.28 @800 nm, 9,11,67,68 and KHC₂O₄·(H₃BO₃) has a value of 0.164@1064 nm. 69 **Li-4HP2** also surpasses most 6-MR compounds, including **4HPP** (0.25@1064 nm), 48 β -(C₃N₆H₇)₂-Cl₂·H₂O (0.38@550 nm), 70 (C₃N₆H₇)₂SiF₆·H₂O (0.152@550 nm), and recently reported C₅H₆NOSb₂OF₄ (0.513@546 nm). 71,72

To gain a deeper understanding of the origin of the giant optical anisotropy in Mg-4HP, the raw reagent Mg(NO₃)₂·6H₂O (ICSD 80446) was selected as a reference. In the structures of Mg(NO₃)₂·6H₂O and Mg-4HP, both coplanar groups (NO₃⁻ and 4HP) are nearly ideally distributed, but with different spatial densities in the lattice (Fig. S18 and S19†). According to DFT calculations, the predicted birefringence of Mg(NO₃)₂·6H₂O is 0.198@546 nm, while Mg-4HP exhibits a larger birefringence of 0.376@546 nm, despite the spatial density of NO₃⁻ (4.02 × 10⁻³ Å⁻³) being nearly half that in Mg-4HP (7.82 × 10⁻³ Å⁻³). This indicates that the 4HP group primarily contributes to the larger birefringence observed in Mg-4HP.

Herein, we establish a model to illustrate the contribution to birefringence from each coplanar group more intuitively. It is well known that the birefringence is related to the density, **Edge Article**

polarizability, and spatial arrangement of the birefringenceactive groups. In other words, Δn is proportional to $\rho \times \Delta \alpha \times \Delta \alpha$ $\cos \theta$, where θ is the dihedral angle between the birefringenceactive groups. To simplify this model, we assume that the large birefringence is solely attributed to the coplanar groups of NO_3^- and 4HP, and the contribution from $[Mg(H_2O)_6]^{2+}$ and [LiO₄H₂O]⁷⁻ polyhedra is almost negligible due to their small $\Delta \alpha$. In Mg(NO₃)₂·6H₂O, NO₃ is the sole birefringence-active group with a nearly parallel arrangement in the lattice. Therefore, it can be used as a benchmark to estimate the contribution to birefringence from the NO₃⁻ and 4HP groups in Mg-4HP. A rough calculation of the contribution to birefringence (@546 nm) from NO₃⁻ in Mg-4HP is approximately $0.198/7.82 \times 4.02 =$ 0.102, indicating that 4HP contributes the remaining 0.274. Interestingly, in Mg-4HP, the ratio of Δn (4HP) to Δn (NO₃⁻) is 2.69, which aligns well with the polarizability results of $\Delta \alpha$ (4HP) to $\Delta \alpha$ (NO₃⁻) = 2.72. This observation highlights the synergistic effect of 4HP and NO₃ in endowing the large birefringence of Mg-4HP. Guided by this idea, the deduced contribution to birefringence (@546 nm) from 4HP and NO₃ is 0.427 and 0.060, and thus the deduced birefringence is 0.487, also

The above model indicates that the giant birefringence of **Li-4HP2** derives from the synergetic effect of the high spatial

contribution to birefringence from each coplanar group.

very close to the measured value of 0.522 (Fig. 6). The slightly

larger margin of error for Li-4HP2 should be related to under-

estimating the distorted $\Delta \alpha$ (NO₃⁻) and not taking the contri-

bution from the distorted [LiO₄H₂O]⁷⁻ polyhedra into account.

However, this simplified model can still be used to reveal the

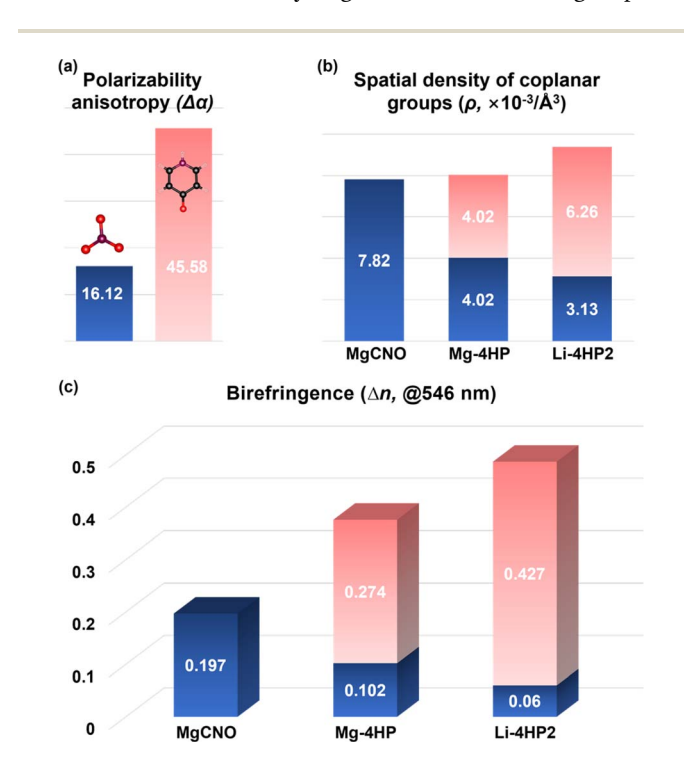


Fig. 6 (a) Polarizability anisotropy ($\Delta\alpha$) of NO $_3^-$ and 4HP. (b) Spatial density (ρ) of coplanar birefringence-active functional building blocks (FBBs) in each compound (blue, NO $_3^-$; red, 4HP, MgNO is Mg(NO $_3$) $_2\cdot$ 6H $_2$ O). (c) Calculated and deduced birefringence (@546 nm) from each coplanar birefringence-active FBB.

density of **4HP** and NO_3^- groups. Interestingly, both **Li-4HP2** and **Mg-4HP** are **4HP-**NO $_3^-$ -based cocrystals, with **4HP** primarily affecting the birefringence. However, the spatial density of **4HP** is increased by nearly 35.8% (from 4.02 in **Mg-4HP** to $6.26 \times 10^{-3} \text{ Å}^{-3}$ in **Li-4HP2**), attributed to the following two reasons: First, in the solution system, Mg^{2+} tends to form the isolated $[Mg(H_2O)_6]^{2+}$ octahedra, where the six water molecules dilute the spatial density of **4HP** in the structure. Second, $[Mg(H_2O)_6]^{2+}$ octahedra can only weakly connect surrounding **4HP** and NO_3^- groups *via* hydrogen bonds, further diluting the spatial density of **4HP**. In contrast, in **Li-4HP2**, Li⁺ connects the **4HP** and NO_3^- *via* stronger covalent Li–O bonds, resulting in a tighter interaction. In addition, the edge-sharing connection in the $[LiNO_3 \cdot H_2O \cdot 4HP]_2$ dimer further increases the spatial density of **4HP** in **Li-4HP2**.

Conclusions

In conclusion, we successfully synthesized two inorganic-organic hybrid cocrystals, Li-4HP2, and Mg-4HP, alongside a by-product, Li-4HP, utilizing a mild aqueous method, resulting in the growth of large crystals. These compounds exhibit substantial bandgaps ranging from 4.08 to 4.51 eV and demonstrate short UV cutoff edges between 275 and 278 nm. The nearly parallel distribution and higher spatial density of coplanar groups contribute to Li-4HP2 displaying a remarkable birefringence of 0.522@546 nm. Our first-principles calculations reveal that the organic 4HP, with its large polarizability, significantly enhances the birefringence observed. Coupled with their ease of growth, short UV cutoff edges, large bandgaps, and impressive birefringence, these compounds emerge as promising candidates for short-wave UV birefringent materials. This study serves as a successful illustration of exploring novel birefringent materials with enhanced birefringence within the cocrystal system.

Data availability

The data that support this article are available within the article and its ESI. \dagger

Author contributions

KMO and YL conceived and designed the project and wrote the manuscript. YL carried out materials synthesis and characterization, as well as performed data analysis. KMO contributed to project administration and funding acquisition. All authors discussed the results and commented on the manuscript.

Conflicts of interest

There are no conflicts to declare.

Acknowledgements

This research was supported by the National Research Foundation of Korea (NRF) funded by the Ministry of Science and ICT (grant no. 2018R1A5A1025208 and 2019R1A2C3005530).

Notes and references

- 1 L. Sun, W. Zhu, X. Zhang, L. Li, H. Dong and W. Hu, *J. Am. Chem. Soc.*, 2021, **143**, 19243–19256.
- 2 S. Aitipamula, R. Banerjee, A. K. Bansal, K. Biradha, M. L. Cheney, A. R. Choudhury, G. R. Desiraju, A. G. Dikundwar, R. Dubey, N. Duggirala, P. P. Ghogale, S. Ghosh, P. K. Goswami, N. R. Goud, R. R. K. R. Jetti, P. Karpinski, P. Kaushik, D. Kumar, V. Kumar, B. Moulton, A. Mukherjee, G. Mukherjee, A. S. Myerson, V. Puri, A. Ramanan, T. Rajamannar, C. M. Reddy, N. Rodriguez-Hornedo, R. D. Rogers, T. N. G. Row, P. Sanphui, N. Shan, G. Shete, A. Singh, C. C. Sun, J. A. Swift, R. Thaimattam, T. S. Thakur, R. Kumar Thaper, S. P. Thomas, S. Tothadi, V. R. Vangala, N. Variankaval, P. Vishweshwar, D. R. Weyna and M. J. Zaworotko, *Cryst. Growth Des.*, 2012, 12, 2147–2152.
- 3 G. R. Desiraju, CrystEngComm, 2003, 5, 466-467.
- 4 D. Yan and D. G. Evans, Mater. Horiz., 2014, 1, 46-57.
- 5 S. Horiuchi, F. Ishii, R. Kumai, Y. Okimoto, H. Tachibana, N. Nagaosa and Y. Tokura, *Nat. Mater.*, 2005, **4**, 163–166.
- 6 L. Sun, Y. Wang, F. Yang, X. Zhang and W. Hu, *Adv. Mater.*, 2019, 31, 1–22.
- 7 G. Bolla, B. Sarma and A. K. Nangia, Chem. Rev., 2022, 122, 11514–11603.
- 8 Y. Wang, W. Zhu, W. Du, X. Liu, X. Zhang, H. Dong and W. Hu, *Angew. Chem., Int. Ed.*, 2018, **57**, 3963–3967.
- 9 X. Meng, K. Kang, Y. Liu, J. Tang, X. Jiang, W. Yin, Z. Lin and M. Xia, *Cryst. Growth Des.*, 2020, **20**, 7588–7592.
- 10 O. Shemchuk, F. Grepioni and D. Braga, *Cryst. Growth Des.*, 2020, **20**, 7230–7237.
- 11 F. Liang, N. Wang, X. Liu, Z. Lin and Y. Wu, *Chem. Commun.*, 2019, 55, 6257–6260.
- 12 Y. Li, X. Chen and K. M. Ok, Chem. Commun., 2022, 3, 3-6.
- 13 H. Wang, L. Liu, Z. Hu, J. Wang, M. Zhu, Y. Meng and J. Xu, *Inorg. Chem.*, 2023, **62**, 557–564.
- 14 Y. Deng, L. Wang, Y. Ge, L. Huang, D. Gao, J. Bi and G. Zou, *Chem. Commun.*, 2020, **56**, 9982–9985.
- 15 H. Tian, C. Lin, X. Zhao, S. Fang, H. Li, C. Wang, N. Ye and M. Luo, *Mater. Today Phys.*, 2022, 28, 100849.
- 16 H. Wu, H. Yu, W. Zhang, J. Cantwell, K. R. Poeppelmeier, S. Pan and P. S. Halasyamani, *Cryst. Growth Des.*, 2017, 17, 4405–4412.
- 17 Q. Wang, L. Wang, X. Zhao, L. Huang, D. Gao, J. Bi, X. Wang and G. Zou, *Inorg. Chem. Front.*, 2019, **6**, 3125–3132.
- 18 Z. Bai and K. M. Ok, Inorg. Chem. Front., 2023, 10, 1919-1925.
- 19 F. Zhang, X. Chen, M. Zhang, W. Jin, S. Han, Z. Yang and S. Pan, *Light: Sci. Appl.*, 2022, 11, 7.
- 20 X. Chen, B. Zhang, F. Zhang, Y. Wang, M. Zhang, Z. Yang, K. R. Poeppelmeier and S. Pan, *J. Am. Chem. Soc.*, 2018, 140, 16311–16319.
- 21 S. Niu, G. Joe, H. Zhao, Y. Zhou, T. Orvis, H. Huyan, J. Salman, K. Mahalingam, B. Urwin, J. Wu, Y. Liu, T. E. Tiwald, S. B. Cronin, B. M. Howe, M. Mecklenburg, R. Haiges, D. J. Singh, H. Wang, M. A. Kats and J. Ravichandran, *Nat. Photonics*, 2018, 12, 392–396.

- 22 P. Li, C. Hu, Y. Li, J. Mao and F. Kong, *J. Am. Chem. Soc.*, 2024, 57, 538–548.
- 23 W. Zeng, Y. Tian, X. Dong, L. Huang, H. Zeng, Z. Lin and G. Zou, *Chem. Mater.*, 2024, **36**, 2138–2146.
- 24 M. J. Dodge, Appl. Opt., 1984, 23, 1980.
- 25 G. Zhou, J. Xu, X. Chen, H. Zhong, S. Wang, K. Xu, P. Deng and F. Gan, *J. Cryst. Growth*, 1998, **191**, 517–519.
- 26 G. Ghosh, Opt. Commun., 1999, 163, 95-102.
- 27 J. R. DeVore, J. Opt. Soc. Am., 1951, 41, 416.
- 28 D. E. Zelmon, D. L. Small and D. Jundt, *J. Opt. Soc. Am. B*, 1997, 14, 3319.
- 29 A. Tudi, S. Han, Z. Yang and S. Pan, Coord. Chem. Rev., 2022, 459, 214380.
- 30 J. Guo, A. Tudi, S. Han, Z. Yang and S. Pan, *Angew. Chem., Int. Ed.*, 2021, **60**, 3540–3544.
- 31 Q. Chen, C. Hu, M. Zhang and J. Mao, *Chem. Sci.*, 2023, **14**, 14302–14307.
- 32 Y. Yang, Y. Xiao, B. Li, Y. Chen, P. Guo, B. Zhang and X. Zhang, J. Am. Chem. Soc., 2023, 145, 22577–22583.
- 33 Y. Liu, X. Liu, S. Liu, Q. Ding, Y. Li, L. Li, S. Zhao, Z. Lin, J. Luo and M. Hong, *Angew. Chem.*, *Int. Ed.*, 2020, 59, 7793–7796.
- 34 M. Liang, Y. Zhang, E. Izvarin, M. J. Waters, J. M. Rondinelli and P. S. Halasyamani, *Chem. Mater.*, 2024, 36, 2113–2123.
- 35 S. Jiang, J. Zhou, H. Wu, H. Yu, Z. Hu, J. Wang and Y. Wu, *Chem. Commun.*, 2020, **56**, 7104–7107.
- 36 X. Wang, M. Xia and R. Li, *Opt. Mater. (Amsterdam, Neth.)*, 2014, 38, 6–9.
- 37 X. Chen, F. Zhang, Y. Shi, Y. Sun, Z. Yang and S. Pan, *Dalton Trans.*, 2018, 47, 750–757.
- 38 X. Liu, L. Kang, P. Gong and Z. Lin, *Angew. Chem., Int. Ed.*, 2021, **60**, 13574–13578.
- 39 Z. Hu, L. Liu, R. Zhang, Q. Jing, H. Wang, J. Tian, J. Xu and P. S. Halasyamani, *J. Mater. Chem. C*, 2023, **1**, 3777.
- 40 H. Sha, B. Li, Z. Xiong, Z. Wang, C. Liu, R. Su, C. He, X. Yang and X. Long, *J. Mater. Chem. C*, 2021, **9**, 15886–15890.
- 41 W. Xiong, L. Chen, L. Huang, F. Guo, Y. Zhou and H. Yuan, *Cryst. Res. Technol.*, 2015, **50**, 250–254.
- 42 R. Li, Z. Kristallogr., 2013, 288, 526-531.
- 43 H. Fan, N. Ye and M. Luo, *Acc. Chem. Res.*, 2023, **56**, 3099–3109.
- 44 Y. Shen, Y. Zhou, X. Xue, H. Yu, S. Zhao and J. Luo, *Inorg. Chem. Front.*, 2022, **21**, 27.
- 45 D. Dou, Q. Shi, Y. Bai, C. Chen, B. Zhang and Y. Wang, *Mater. Chem. Front.*, 2023, 7, 5924–5931.
- 46 J. Lu, Y. Lian, L. Xiong, Q. Wu, M. Zhao, K. Shi, L. Chen and L. Wu, *J. Am. Chem. Soc.*, 2019, **141**, 16151–16159.
- 47 X. Liu, P. Gong and Z. Lin, *Inorg. Chem.*, 2021, **60**, 10890–10894.
- 48 J. Lu, X. Liu, M. Zhao, X. Deng, K. Shi, Q. Wu, L. Chen and L. Wu, *J. Am. Chem. Soc.*, 2021, **143**, 3647–3654.
- 49 Z. Zhang, X. Liu, X. Liu, Z. Lu, X. Sui, B. Zhen, Z. Lin, L. Chen and L. Wu, *Chem. Mater.*, 2022, 34, 1976–1984.
- 50 X. Liu, P. Gong and Z. Lin, *Inorg. Chem.*, 2021, **60**, 10890– 10894
- 51 SAINT, version 7.60A, Bruker Analytical X-Ray Instruments Inc., Madison, WI, 2008.

Edge Article Chemical Science

- 52 O. V. Dolomanov, L. J. Bourhis, R. J. Gildea, J. A. K. Howard and H. Puschmann, J. Appl. Crystallogr., 2009, 42, 339-341.
- 53 A. L. Spek, J. Appl. Crystallogr., 2003, 36, 7-13.
- 54 M. J. Frisch, et al., Gaussian 09, Revision D.01, Gaussian, Inc. Wallingford CT, 2009.
- 55 T. Lu and F. Chen, J. Comput. Chem., 2012, 33, 580-592.
- 56 T. D. Kühne, M. Iannuzzi, M. Del Ben, V. V. Rybkin, P. Seewald, F. Stein, T. Laino, R. Z. Khaliullin, O. Schütt, F. Schiffmann, D. Golze, J. Wilhelm, S. Chulkov, Bani-Hashemian, V. Weber, U. Borštnik, M. M. Taillefumier, A. S. Jakobovits, A. Lazzaro, H. Pabst, Müller, R. Schade, M. Guidon, S. Andermatt, Holmberg, G. K. Schenter, A. Hehn, A. Bussy, F. Belleflamme, G. Tabacchi, A. Glöß, M. Lass, I. Bethune, C. J. Mundy, C. Plessl, M. Watkins, J. VandeVondele, M. Krack and J. Hutter, J. Chem. Phys., 2020, 152, 194103.
- 57 S. J. Clark, M. D. Segall, C. J. Pickard, P. J. Hasnip, M. I. J. Probert, K. Refson and M. C. Payne, Z. Kristallogr.-Cryst. Mater., 2005, 220, 567-570.
- 58 W. Wang, H. Fan and Y. Ye, Polymer (Guildf)., 2010, 51, 3575-3581.
- 59 J. P. Perdew, K. Burke and M. Ernzerhof, Phys. Rev. Lett., 1996, 77, 3865-3868.
- 60 K. Liu, H. Fan, P. Ren and C. Yang, J. Alloys Compd., 2011, 509, 1901-1905.

- 61 J. Lin, A. Qteish, M. C. Payne and V. Heine, Phys. Rev. B: Condens. Matter Mater. Phys., 1993, 47, 4174.
- 62 M. Mutailipu, X. Su, M. Zhang, Z. Yang and S. Pan, Inorg. Chem. Front., 2017, 4, 281-288.
- 63 R. A. Nyquist and R. O. Kagel, Infrared Spectra of Inorganic Compounds, Elsevier, 1971.
- 64 X. Pan, H. Wu, S. Cheng and Z. Wang, Inorg. Chem. Front., 2019, 7, 101-107.
- 65 H. Luo, T. Tkaczyk, R. Sampson and E. L. Dereniak, Semiconductor Photodetectors III, 2006, vol. 6119, 61190J.
- 66 X. Hao, M. Luo, C. Lin, G. Peng, T. Yan, D. Lin, L. Cao, X. Long, G. Yang and N. Ye, Inorg. Chem., 2020, 59, 10361-10367.
- 67 J. Wang, X. Zhang, F. Liang, Z. Hu and Y. Wu, Cryst. Growth Des., 2021, 21, 7194-7200.
- 68 J. Wang, X. Zhang, F. Liang, Z. Hu and Y. Wu, Dalton Trans., 2021, 50, 11555-11561.
- 69 Y. Li, J. Lee and K. M. Ok, Bull. Korean Chem. Soc., 2023, 1-6.
- 70 Y. Shen, L. Ma, G. Dong, H. Yu and J. Luo, Inorg. Chem. Front., 2023, 22, 12-14.
- 71 Y. Shen, Y. Zhou, X. Xue, H. Yu, S. Zhao and J. Luo, Inorg. Chem. Front., 2022, 9, 5226-5230.
- 72 L. Qi, X. Jiang, K. Duanmu, C. Wu, Z. Lin, Z. Huang, M. G. Humphrey and C. Zhang, J. Am. Chem. Soc., 2024, 146, 9975-9983.